SCIENCE CHINA Materials ARTICLES

mater.scichina.com link.springer.com

Published online 21 October 2020 | https://doi.org/10.1007/s40843-020-1469-2
Sci China Mater 2021, 64(3): 601–610

Surface-structure tailoring of ultrafine PtCu nanowires for enhanced electrooxidation of alcohols

Liping Huang[1,2†], Wei Zhang[3,4†], Yanfei Zhong[1,2†], Peng Li[1,2*], Dong Xiang[1], Waqar Uddin[1], Xiaowu Li[1], Yang-Gang Wang[3*], Xiaoyou Yuan[1], Dingsheng Wang[5] and Manzhou Zhu[1,2*]

ABSTRACT **Surface tailoring of Pt-based nanocatalysts is an effective pathway to promote their electrocatalytic performance and multifunctionality. Here, we report two kinds of one-dimensional (1D) ultrafine PtCu nanowires (smooth surface & rugged surface) synthesized *via* a wet chemical method and their distinct catalytic performances in electrooxidation of alcohols. The alloyed PtCu nanowires having rough surfaces with atomic steps exhibit superior catalytic activity toward multiple electrochemical reactions compared with the smooth counterpart. Density functional theory simulations show the excellent reactivity of rugged PtCu nanowires and attribute it to the surface synergetic Pt-Cu site which accounts for the promotion of water dissociation and the dehydrogenation of the carboxyl intermediate. The current study provides an insight into reasonable design of alloy nanocatalysts in energy-related electrocatalytic systems.**

Keywords: PtCu nanowires, surface tailoring, high-index facets, alcohol oxidation, ultrafine

INTRODUCTION

A large variety of energy-related electrocatalytic systems have attracted widespread attention [1–3], such as electrochemical alcohol oxidation reactions (EAOR), oxygen reduction reaction (ORR), and hydrogen evolution reaction (HER) [4–17]. Platinum is one of the most effective monometallic electrocatalysts in acidic media due to its superior catalytic nature [18]. However, the low abundance and CO poisoning of platinum catalysts remain a huge challenge [19]. The use of alloying with transition metals has achieved Pt-based bimetallic or multimetallic electrocatalysts that enable significantly improved activity and durability [20–39]. Meanwhile, precisely controlled fabrication of Pt-based alloys with tailored facets and compositions can not only improve the utilization efficiency of Pt, but also modify the electronic and geometric structures, thus benefiting for achieving higher catalytic activities [40–43]. Recently, Feng and co-workers [44] demonstrated that bimetallic PtCu alloyed nanocages with high-index facets exhibited enhanced catalytic activities toward oxygen reduction and polyhydric alcohol oxidation. Remarkably, massive studies show that one-dimensional (1D) nanowires (NWs) exhibit enhanced electrocatalytic activity owing to their large surface area, high surface electron conductivity, surface defects, and abundant unique quantum effects [45–53]. For example, Dong and co-works [54] reported that PtRu NWs exhibited much higher performance toward alcohol oxidation reactions as compared with PtRu nanocubes (NCs). Designing 1D Pt-based nanocatalyst with high-indexed facets is also an effective way to promote the catalytic performance, in which atoms at the steps, edges and bends may serve as the active sites for catalysis [55–59]. For instance, Huang's group [60,61] demonstrated that Pt nanocrystals with high-index {411} facets and screw thread-like PtCu NWs had excellent electrocatalytic activities. Therefore, rational preparation of shape-con-

[1] Department of Chemistry and Centre for Atomic Engineering of Advanced Materials, Anhui Province Key Laboratory of Chemistry for Inorganic/Organic Hybrid Functionalized Materials, Hefei 230601, China
[2] Key Laboratory of Structure and Functional Regulation of Hybrid Materials (Anhui University), Ministry of Education, Hefei 230601, China
[3] Department of Chemistry and Guangdong Provincial Key Laboratory of Catalytic Chemistry, Southern University of Science and Technology, Shenzhen 518055, China
[4] College of Civil Engineering & Mechanics, Xiangtan University, Xiangtan 411105, China
[5] Department of Chemistry, Tsinghua University, Beijing 100084, China
† These authors contributed equally to this work.
* Corresponding authors (emails: peng-li@ahu.edu.cn (Li P); wangyg@sustech.edu.cn (Wang YG); zmz@ahu.edu.cn (Zhu M))

trollable nanocatalysts is of great significance to the improvement of catalytic performance.

In this work, we report two kinds of 1D ultrafine PtCu NWs (smooth surface & rugged surface) synthesized by using a wet-chemical approach. Interestingly, the rugged PtCu NWs exhibit superior electrocatalytic activities toward the EAOR in comparison with smooth PtCu NWs and commercial Pt/C. As evidenced by a series of characterizations, the enhanced catalytic performance of rugged PtCu NWs is ascribed to their abundant atomic steps that serve as the active sites and higher content of Cu, resulting in the superior intrinsic activity.

EXPERIMENTAL SECTION

Chemicals

Platium(II) acetylacetonate ($Pt(acac)_2$), cupricchloride dihydrate ($CuCl_2{\cdot}2H_2O$), hexacarbonyltungsten ($W(CO)_6$), glucose ($C_6H_{12}O_6$), dodecyl trimethyl ammonium bromide (DTAB), oleylamine (OAm), 1-octadecene (ODE), cyclohexane (C_6H_{12}), acetic acid (CH_3COOH), ethanol (CH_3CH_2OH), methanol (CH_3OH), and Vulcan XC-72 carbon were used as received. Deionized (DI) water was used for all aqueous solutions.

Synthesis of smooth PtCu NWs

In a typical synthesis, $Pt(acac)_2$ (10 mg), $W(CO)_6$ (1.8 mg), glucose (16.7 mg) and DTAB (15.8 mg) were mixed with OAm (3 mL) and ODE (2 mL) in a vial (30 mL). After sonication for 25 min, the obtained solution was heated up to 170°C and maintained for 0.5 h in an oil bath. Then $CuCl_2{\cdot}2H_2O$ (2.1 mg) dissolved in OAm (1 mL) and ODE (1 mL) was added into the above solution under magnetic stirring and maintained at 170°C for 5.5 h. Finally, the products were cooled down to ambient temperature, collected by centrifugation and washed several times with an ethanol/cyclohexane mixture.

Synthesis of rugged PtCu NWs

In a typical synthesis, $Pt(acac)_2$ (10 mg), glucose (16.7 mg) and DTAB (15.8 mg) were mixed with OAm (3 mL) and ODE (2 mL) in a vial (30 mL). After sonication for 25 min, the obtained solution was heated up to 170°C and maintained for 0.5 h. Then $CuCl_2{\cdot}2H_2O$ (2.1 mg) dissolved in OAm (1 mL) and ODE (1 mL) was added into the above solution under magnetic stirring and maintained at 170°C for 5.5 h. Finally, the products were cooled down to ambient temperature, collected by centrifugation and washed several times with an ethanol/cyclohexane mixture.

Preparation of the PtCu/C catalysts

The PtCu nanocatalysts (5 mg) dispersed in cyclohexane (10 mL) were mixed with Vulcan XC-72 carbon (15 mg), and sonicated for 1 h. The resulting PtCu/C catalysts were collected by centrifugation, washed with ethanol and acetic acid, and dried overnight in a fume hood.

Characterization

Transmission electron microscopy (TEM), high-resolution TEM (HRTEM), energy dispersive spectrometer (EDS) and EDS elemental mappings of PtCu NWs were performed on a JEOL JEM-2010 transmission electron microscope operating at 200 kV. High-angle annular dark-field scanning transmission electron microscopy (HAADF-STEM) measurements were conducted with an FEI Themis Z transmission electron microscope operating at 300 kV. The X-ray diffraction (XRD) analysis was recorded on Smart Lab 9 KW using Cu-Kα radiation. The Pt and Cu contents in the PtCu catalysts were determined by inductively coupled plasma optical emission spectroscopy (ICP-OES). X-ray photoelectron spectroscopy (XPS) characterization was carried out on a Thermo ESCALAB 250 with Al-Kα radiation.

Electrochemical measurements

Electrochemical measurements were performed using a three-electrode system with a CHI 660E electrochemical workstation at room temperature. Glassy carbon (GC) disk electrode (5 mm, 0.196 cm^2) was used as the working electrode. A KCl-saturated Ag/AgCl electrode was taken as the reference electrode and Pt sheet was used as the counter electrode in acidic media. A leak-free Hg/HgO electrode was taken as the reference electrode and Graphite electrode was used as the counter electrode in alkaline media. A moderate amount of PtCu/C catalysts were dispersed in mixed solution containing 480 μL ethanol and 20 μL Nafion (5%). The suspension of PtCu/C catalysts with the volume of 20 μL (0.25 mg_{Pt} mL^{-1}) was pipetted on the surface of GC and dried at ambient temperature. Commercial Pt/C (20%) catalysts were used as the contrast catalyst during the electrochemical test.

RESULTS

The PtCu NWs with smooth surfaces were obtained by a simple wet-chemical, and two-step synthetic process. PtCu NWs with the rugged surfaces were also obtained in the absence of $W(CO)_6$ through the similar synthetic process (Scheme 1, see EXPERIMENTAL SECTION for details).

TEM images reveal that PtCu NWs with different

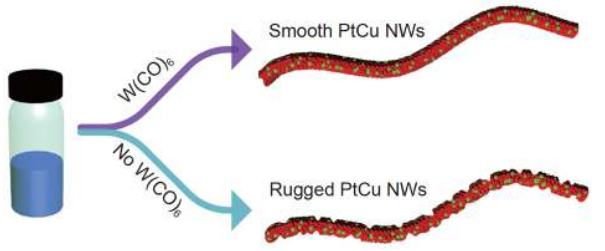

Scheme 1 Schematic diagram of the synthetic route to PtCu NWs with variable atomic surfaces and compositions.

atomic surfaces and compositions have been synthesized (Figs 1a and 2a). Generally, the as-prepared PtCu NWs are monodisperse and with a high synthetic yield. As shown in Fig. 1b, the as-obtained PtCu NWs have smooth surfaces with an average diameter of 3 nm. The inset shows the corresponding fast Fourier transform (FFT) pattern in the [001] orientation, indicating the growth of the as-prepared NWs along <110> direction and the side surface parallel to (220). Meanwhile, the (200) side facets were also observed in different orientations (Fig. S1a). Therefore, the results demonstrate that the as-obtained smooth PtCu NWs predominantly expose their (220) and (200) facets. When no $W(CO)_6$ was added, keeping all other experimental conditions unchanged, PtCu NWs with stepped surfaces were further obtained. The representative TEM image (Fig. 2a) shows that the average diameter of the rugged PtCu NWs is about 4 nm. Importantly, the side surface of the as-prepared PtCu NWs is not smooth. Characteristically, the HAADF-STEM image presents the {111} facets and a high density of low-coordinate surface steps, such as the (511) surface (Fig. 2b and Fig. S1b).

The EDS mapping profile was also conducted to manifest Pt and Cu elements in both smooth and rugged PtCu NWs (Figs 1c and 2c), indicating their uniform distributions around the 1D PtCu nanostructures. Meanwhile, the Pt/Cu atomic ratio of smooth PtCu NWs (69.8%/30.2%) was measured by EDS (Fig. S2a), which is in accordance with the results determined by ICP-OES (71.6%/28.4%). For comparison, the EDS spectrum (Fig. S2b) indicates that the atomic ratio of Pt/Cu for the rugged PtCu NWs is 54.1%/45.9%, similar to that by ICP-OES (53.2%/46.8%). It is evident that the Cu content of rugged PtCu NWs is significantly higher than that of smooth PtCu NWs. But no obvious W element was detected in the smooth PtCu NWs, possibly because W $(CO)_6$ was only used as a powerful reductant for Pt and Cu precursors.

To further investigate their structures, XRD characterization for the smooth and rugged PtCu NWs was conducted (Fig. 3a). The XRD peak positions of the as-obtained products are between Pt and Cu standard card, which suggests that both PtCu NWs have face-centered cubic (fcc) alloy structure. In addition, the element valence of both PtCu NWs was analyzed by XPS (Fig. 3b and c). Compared with pure Pt, the XPS results show that the Pt $4f_{7/2}$ peaks (Pt^0) of the PtCu NWs catalysts shift to a higher binding energy because of the incorporation of Cu atoms [62]. And the positions of Cu 2p peak and Pt 4f peak for both PtCu NWs are almost identical. In addition,

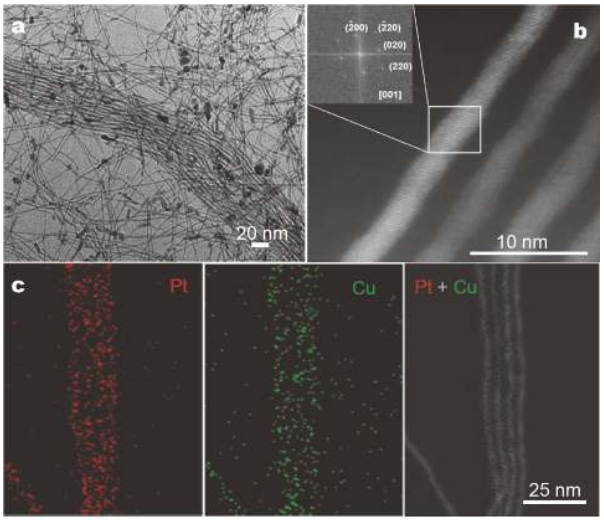

Figure 1 TEM image (a), HAADF-STEM image (b) (inset shows the corresponding FFT pattern), and EDS elemental mapping images (c) of the smooth PtCu NWs (Pt: red, Cu: green).

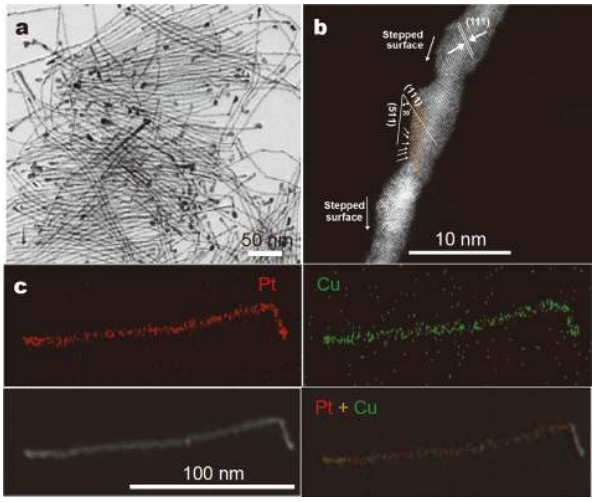

Figure 2 TEM image (a), HAADF-STEM image (b), and EDS elemental mapping images (c) of the rugged PtCu NWs (Pt: red, Cu: green).

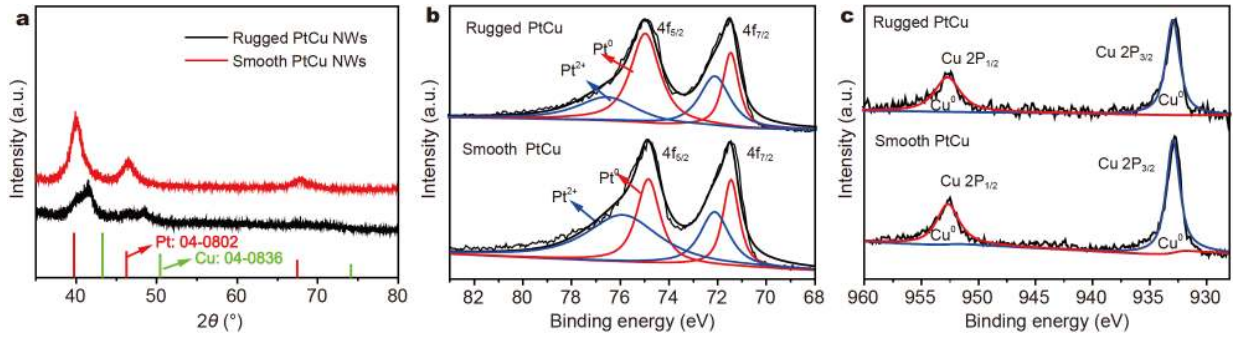

Figure 3 (a) XRD patterns of smooth and rugged PtCu NWs. XPS valence band structure of (b) Pt and (c) Cu.

platinum and copper have the same valence state in both PtCu NWs.

In order to clarify the formation mechanism of PtCu NWs, the morphologies of the intermediates at different reaction times were investigated by TEM. Fig. 4a and d display that pure Pt NWs were formed in the initial reaction stage. After 0.5 h of reaction at 170°C, ultrathin Pt NWs with an average size of ~1 nm could be obtained. Glucose and DTAB may play cooperative structure-directing roles in the growth of 1D Pt nanostructures. Note that the as-obtained 1-nm-thick Pt NWs may be divided into short NWs under high intensity electron beam irradiation, due to its atom-level thickness [63]. After 1 h of reaction, the addition of $CuCl_2{\cdot}2H_2O$ in the reaction system could lead to PtCu NWs instead of Pt NWs (Fig. 4b and e). The difference between the reduction potentials of platinum and copper precursors may lead to the reduction and diffusion of Cu species, eventually forming alloyed PtCu NWs. When the reaction time was further prolonged to 2.5 h (Fig. 4c), small clumps began to grow on the surface and the diameter of the rugged PtCu NWs became ~3 nm, similar to the final product. With the increase of reaction time, the rugged surface structure became obvious. With the extended reaction time, the average diameter of smooth PtCu NWs also increases (Fig. 4d–f). When the reaction time reached 2.5 h, the average diameter of the obtained NWs increased to ~2 nm (Fig. 4f). Notably, the as-synthesized PtCu NWs are always thinner than the rugged NWs, and the surface remains smooth. The results indicate that $W(CO)_6$ is vital for the nucleation and growth of PtCu NWs. The absence of $W(CO)_6$ might reduce the nucleation rates of Pt^{2+} and Cu^{2+} ions, leading to the growth of rugged PtCu NWs with high-indexed stepped surfaces. However, the in-

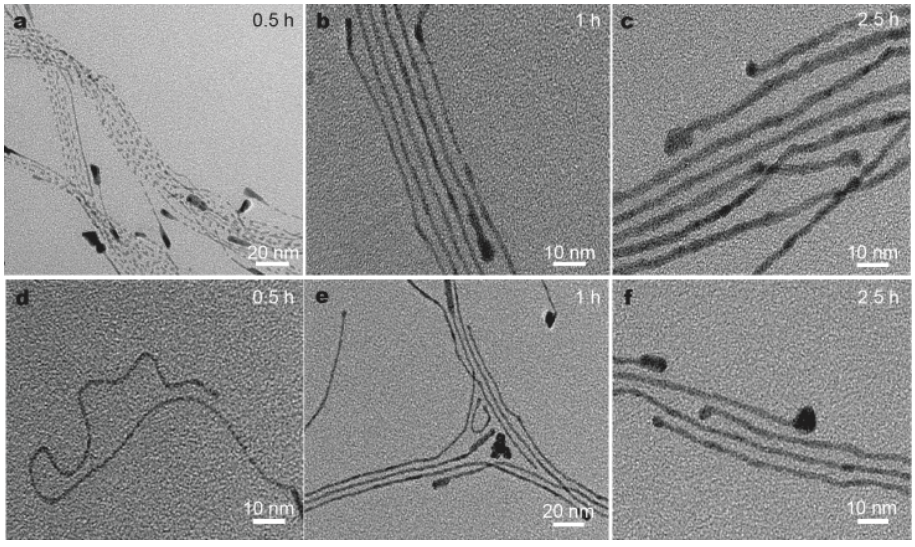

Figure 4 Growth process for the unique PtCu NWs. Typical TEM images of rugged PtCu NWs (a–c) and smooth PtCu NWs (d–f) formed at different reaction times, respectively.

troduction of $W(CO)_6$ enables the precursors to grow into the PtCu NWs with smooth surfaces.

Electrocatalytic activities of the as-prepared PtCu NWs toward EAOR were further evaluated by cyclic voltammetry (CV) curves in comparison with the commercial Pt/C. Fig. S3 compares the CVs on these three different catalysts recorded in N_2-saturated 0.5 mol L^{-1} H_2SO_4 solution at a sweep rate of 100 mV s^{-1}. The electrochemically active surface areas (ECSAs) calculated by integrating the hydrogen-adsorption charge were 31.3 m^2 g_{Pt}^{-1} for the rugged PtCu NWs, 25.9 m^2 g_{Pt}^{-1} for the smooth PtCu NWs, and 64.3 m^2 g_{Pt}^{-1} for commercial Pt/C.

The methanol oxidation reactions (MORs) of rugged PtCu NWs, smooth PtCu NWs and commercial Pt/C were measured in 0.5 mol L^{-1} H_2SO_4 + 1 mol L^{-1} CH_3OH at room temperature with a sweep rate of 50 mV s^{-1}. As shown in Fig. 5a and b, both the as-prepared catalysts show better separation peaks than those of commercial Pt/C in the processes of forward and reverse sweeps. The rugged and smooth PtCu NWs exhibit specific activities of 4.39 and 2.26 mA cm^{-2}, respectively, which are 9.15 and 4.71 times greater than that of commercial Pt/C (0.48 mA cm^{-2}). Similarly, the mass activity reaches 1.03 and 0.72 A mg_{Pt}^{-1} for the rugged and smooth PtCu NWs, which are 3.32 and 2.32 times higher than that of commercial Pt/C (0.31 A mg_{Pt}^{-1}), respectively (Fig. 5c). Specific and mass activities of both PtCu NWs were significantly higher than those of commercial Pt/C, indicating that the 1D bimetallic nanostructures significantly improved the electrochemical properties. To evaluate the MOR stability of the three catalysts, chronoamperometry (CA) curves were conducted at 0.8 V *vs.* RHE for 2000 s (Fig. S4a). Specifically, rugged PtCu NWs and corresponding smooth PtCu NWs exhibited better durability than commercial Pt/C.

In addition, the electrocatalytic performances of the three catalysts in the ethanol oxidation (EtOR) were evaluated in 0.5 mol L^{-1} H_2SO_4 + 2 mol L^{-1} CH_3CH_2OH solutions at a sweeping rate of 50 mV s^{-1}. As shown in Fig. 5d and e, the rugged PtCu NWs display the highest ethanol oxidation current density compared with smooth PtCu NWs and commercial Pt/C. The specific activity of rugged PtCu NWs (5.12 mA cm^{-2}) at 0.98 V (*vs.* RHE) is 1.64 and 4.10 times greater than those of smooth PtCu NWs (3.12 mA cm^{-2}) and commercial Pt/C (1.25 mA cm^{-2}), respectively. And the rugged PtCu NWs also possess the highest mass activity of 1.31 A mg_{Pt}^{-1}, which is 1.62 and 1.82 times higher than those of the smooth PtCu NWs (0.81 A mg_{Pt}^{-1}) and commercial Pt/C (0.72 A mg_{Pt}^{-1}), respectively (Fig. 5f). To further investigate the electrocatalytic stability of EtOR, CA curves

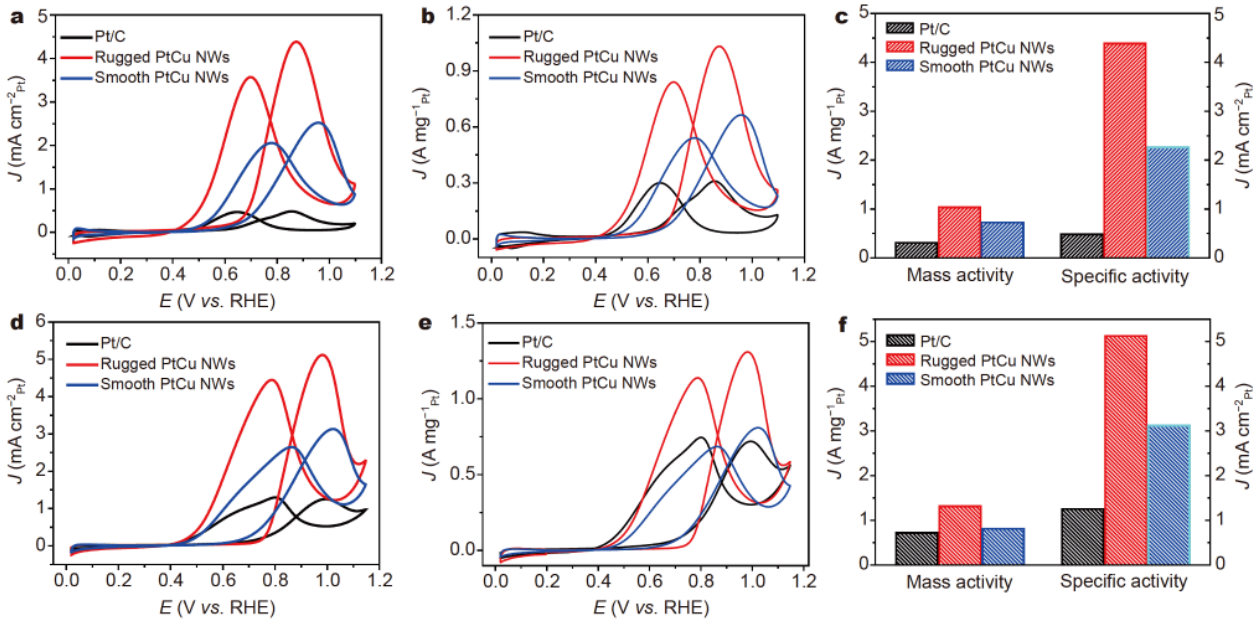

Figure 5 (a, b) CV curves of the rugged PtCu NWs, smooth PtCu NWs and commercial Pt/C in a solution of 0.5 mol L^{-1} H_2SO_4 + 1 mol L^{-1} CH_3OH at 50 mV s^{-1} (a, forward sweep; b, reverse sweep); (c) histogram of mass and specific activities of different catalysts for methanol oxidation; (d, e) CV curves of the rugged PtCu NWs, smooth PtCu NWs and commercial Pt/C in a solution of 0.5 mol L^{-1} H_2SO_4 + 2 mol L^{-1} CH_3CH_2OH at 50 mV s^{-1} (d, forward sweep; e, reverse sweep); (f) histogram of mass and specific activities of different catalysts for ethanol oxidation.

were obtained at 0.85 V (*vs.* RHE) for 2000 s (Fig. S4b). As we can seen, the rugged PtCu NWs possess excellent durability during the whole electrochemical measurements, in comparison with smooth PtCu NWs and commercial Pt/C. The experimental results confirm that the electrochemical performance of the catalysts is significantly enhanced by 1D bimetallic NWs.

Moreover, we then evaluated the HER performances of these electrocatalysts. Fig. S5 displays the linear sweep voltammetry (LSV) curves of the electrocatalysts conducted in 1 mol L^{-1} KOH aqueous solution at the scanning rate of 5 mV s^{-1}. The performance of rugged PtCu NWs is greater than that of smooth PtCu NWs and commercial Pt/C.

After electrochemical testing, the rugged and smooth PtCu NWs were collected from the electrodes and further characterized by TEM and HRTEM. The results show that there are no noticeable structural and morphological changes (Fig. S6). As discussed above, these experimental results demonstrate the enhanced electrocatalytic performance of rugged PtCu NWs for MOR, EtOR and HER compared with those of smooth PtCu NWs and commercial Pt/C.

DISCUSSION

To reveal the mechanistic nature of electro-oxidation over PtCu NWs, we performed density functional theory (DFT) simulations on MOR over PtCu(100), (110), (111) and (511) surface models (Fig. S7). The former two surfaces were mainly observed on the smooth NWs and the latter two on the rugged NWs. As reported in previous studies [64,65], the general pathway for methanol electro-oxidation was considered to include the following seven elementary steps, (i) $*CH_3OH \rightarrow *CH_2OH + H^+ + e^-$; (ii) $*CH_2OH \rightarrow *CHOH + H^+ + e^-$; (iii) $*CHOH \rightarrow HCO*$ (or $*COH$) $+ H^+ + e^-$; (iv) $HCO*$(or $*COH$) $\rightarrow *CO + H^+ + e^-$; (v) $H_2O* \rightarrow *OH + H^+ + e^-$; (vi) $*CO + *OH \rightarrow *COOH$; (vii) $*COOH \rightarrow CO_2 + H^+ + e^-$, where (i)–(iv) are the direct dehydrogenation steps of methanol, (v) denotes the water dissociation step, (vi) is the combination of *CO with *OH, and (vii) is the dehydrogenation of carboxyl intermediate *COOH to release CO_2. It is noted that steps (i)–(v) and (vii) are the proton coupled electron transfer (PCET) steps, and step (vi) is a thermodynamic step. In our calculations, we assume that for PCET step the electrochemical driving force (i.e., the applied potential) is needed if its free energy change is

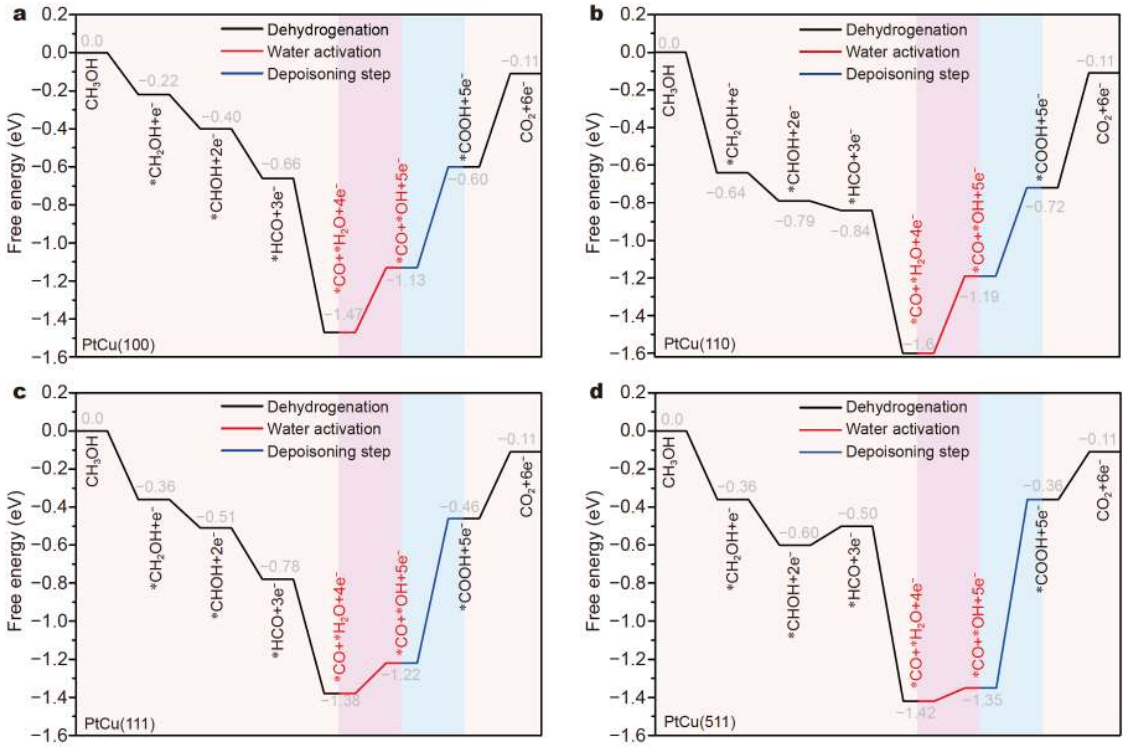

Figure 6 Reaction free energy pathways for methanol oxidation over (a) PtCu(100), (b) PtCu(110), (c) PtCu(111), and (d) PtCu(511) at pH 0 and 300 K. Black, red and blue lines represent the dehydrogenation steps, water dissociation, and the depoisoning step (i.e., the combination of *CO + *OH), respectively.

positive, while for the thermodynamic step the reaction could proceed if the kinetic barrier can be overcome under the experimental temperature. Based on this assumption, we could conclude that the PCET steps mainly determine the observed potential and the thermodynamic step is possible to affect the kinetics during methanol electrooxidation.

The free-energy pathways at U=0 V under the standard condition are shown in Fig. 6. The configurations of reaction intermediates and detail energetics can be found in Fig. S8 and Tables S1–S4. On the basis of the obtained free energy pathways, it can be found that water dissociation and the dehydrogenation of carboxyl intermediate (*COOH) are the dominant energy-rising PCET steps which should determine the overpotential of methanol oxidation. The potentials needed to drive the water splitting ($H_2O \rightarrow OH + H^+ + e^-$) are calculated to be 0.34, 0.41, 0.16 and 0.07 V for (100), (110), (111) and (511), respectively. Similarly, the dehydrogenation of carboxyl intermediates requires additional potentials of 0.49, 0.61, 0.35 and 0.25 V for each surface. These results suggest that (111) and (511) surfaces should exhibit better performance for water dissociation and the carboxyl dehydrogenation. For the configurations of reaction intermediates, it is found that the *CO intermediate strongly adsorb at the Pt site on each surface, which is usually considered as CO poisoning on Pt electrode. Fortunately, with the presence of Cu, water is always activated at the Cu site, forming an active hydroxyl intermediate *OH near the *CO. As a result, the combination of *CO with *OH to form the carboxyl intermediate at the synergetic Pt-Cu sites is the key thermodynamic step for the depoisoning of the stable *CO. We thus also calculated the kinetic barriers for each surface model as shown in Fig. 7. All the barriers are less than 1.10 eV with the lowest one (0.72 eV) on (111) surface. Based on the transition state theory, the energy barriers are expected to be overcome under the experimental temperature (170°C). Overall, it is concluded that the rugged NWs should exhibit higher reactivity toward methanol electrooxidation than the smooth ones, and the high reactivity is attributed to the synergetic Pt-Cu site for promoting water dissociation and carboxyl dehydrogenation.

CONCLUSIONS

In summary, we have successfully synthesized smooth and rugged PtCu NWs by regulating the type of precursor. The rugged PtCu NWs with surface steps exhibit enhanced electrocatalytic activities toward EAOR, compared with smooth PtCu NWs and commercial Pt/C. The DFT calculations also show that the rugged PtCu exhibit much higher reactivity toward methanol oxidation, and the catalytic nature probably originates from the synergetic Pt-Cu site which accounts for the water dissociation and carboxyl dehydrogenation. This work reports a catalyst with evident electrocatalytic performance, which has broad application prospects in energy-related electrocatalytic systems.

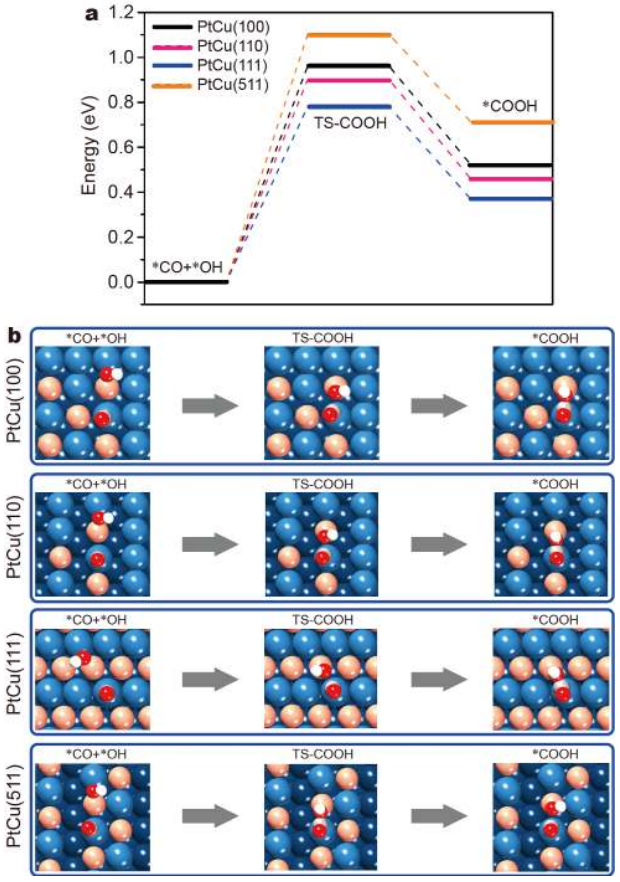

Figure 7 The energy paths for the combination of *CO and *OH (a) and the corresponding configurations (b) on PtCu surfaces.

Received 4 June 2020; accepted 22 July 2020; published online 21 October 2020

1 Zhang Q, Liu J, Xia T, *et al.* Antiferromagnetic element Mn modified PtCo truncated octahedral nanoparticles with enhanced activity and durability for direct methanol fuel cells. Nano Res, 2019, 12: 2520–2527

2 Wang YJ, Zhao N, Fang B, *et al.* Carbon-supported Pt-based alloy electrocatalysts for the oxygen reduction reaction in polymer electrolyte membrane fuel cells: particle size, shape, and composition manipulation and their impact to activity. Chem Rev, 2015, 115: 3433–3467

3 Antolini E. Alloy *vs.* intermetallic compounds: Effect of the ordering on the electrocatalytic activity for oxygen reduction and the stability of low temperature fuel cell catalysts. Appl Catal B-Environ, 2017, 217: 201–213
4 Luo Z, Tan C, Lai Z, *et al.* A simple electrochemical method for conversion of Pt wires to Pt concave icosahedra and nanocubes on carbon paper for electrocatalytic hydrogen evolution. Sci China Mater, 2019, 62: 115–121
5 Zhao Z, Liu H, Gao W, *et al.* Surface-engineered PtNi-O nanostructure with record-high performance for electrocatalytic hydrogen evolution reaction. J Am Chem Soc, 2018, 140: 9046–9050
6 Meng Z, Xiao F, Wei Z, *et al.* Direct synthesis of L10-FePt nanoparticles from single-source bimetallic complex and their electrocatalytic applications in oxygen reduction and hydrogen evolution reactions. Nano Res, 2019, 12: 2954–2959
7 Hong W, Wang J, Wang E. Facile synthesis of PtCu nanowires with enhanced electrocatalytic activity. Nano Res, 2015, 8: 2308–2316
8 Zhao Z, Chen C, Liu Z, *et al.* Pt-based nanocrystal for electrocatalytic oxygen reduction. Adv Mater, 2019, 31: 1808115
9 Wang P, Jiang K, Wang G, *et al.* Phase and interface engineering of platinum-nickel nanowires for efficient electrochemical hydrogen evolution. Angew Chem Int Ed, 2016, 55: 12859–12863
10 Yang J, Wang X, Li B, *et al.* Novel iron/cobalt-containing polypyrrole hydrogel-derived trifunctional electrocatalyst for self-powered overall water splitting. Adv Funct Mater, 2017, 27: 1606497
11 Wang Q, Zhao Z, Jia Y, *et al.* Unique Cu@CuPt core–shell concave octahedron with enhanced methanol oxidation activity. ACS Appl Mater Interfaces, 2017, 9: 36817–36827
12 Zhang J, Chen Z, Liu C, *et al.* Hierarchical iridium-based multimetallic alloy with double-core-shell architecture for efficient overall water splitting. Sci China Mater, 2020, 63: 249–257
13 Wu F, Zhang L, Lai J, *et al.* PtCu–O highly excavated octahedral nanostructures built with nanodendrites for superior alcohol electrooxidation. J Mater Chem A, 2019, 7: 8568–8572
14 Li W, Hu ZY, Zhang Z, *et al.* Nano-single crystal coalesced PtCu nanospheres as robust bifunctional catalyst for hydrogen evolution and oxygen reduction reactions. J Catal, 2019, 375: 164–170
15 Xue S, Deng W, Yang F, *et al.* Hexapod PtRuCu nanocrystalline alloy for highly efficient and stable methanol oxidation. ACS Catal, 2018, 8: 7578–7584
16 Bao M, Amiinu IS, Peng T, *et al.* Surface evolution of PtCu alloy shell over Pd nanocrystals leads to superior hydrogen evolution and oxygen reduction reactions. ACS Energy Lett, 2018, 3: 940–945
17 Fu QQ, Li HH, Ma SY, *et al.* A mixed-solvent route to unique PtAuCu ternary nanotubes templated from Cu nanowires as efficient dual electrocatalysts. Sci China Mater, 2016, 59: 112–121
18 Lu Y, Wang W, Chen X, *et al.* Composition optimized trimetallic PtNiRu dendritic nanostructures as versatile and active electrocatalysts for alcohol oxidation. Nano Res, 2019, 12: 651–657
19 Yuan X, Jiang X, Cao M, *et al.* Intermetallic PtBi core/ultrathin Pt shell nanoplates for efficient and stable methanol and ethanol electro-oxidization. Nano Res, 2019, 12: 429–436
20 Li M, Zhao Z, Cheng T, *et al.* Ultrafine jagged platinum nanowires enable ultrahigh mass activity for the oxygen reduction reaction. Science, 2016, 354: 1414–1419
21 Zheng X, Cao Y, Han X, *et al.* Pt embedded Ni_3Se_2@NiOOH core-shell dendrite-like nanoarrays on nickel as bifunctional electrocatalysts for overall water splitting. Sci China Mater, 2019, 62: 1096–1104
22 Lu Y, Thia L, Fisher A, *et al.* Octahedral PtNi nanoparticles with controlled surface structure and composition for oxygen reduction reaction. Sci China Mater, 2017, 60: 1109–1120
23 Gocyla M, Kuehl S, Shviro M, *et al.* Shape stability of octahedral PtNi nanocatalysts for electrochemical oxygen reduction reaction studied by *in situ* transmission electron microscopy. ACS Nano, 2018, 12: 5306–5311
24 Chen G, Xu C, Huang X, *et al.* Interfacial electronic effects control the reaction selectivity of platinum catalysts. Nat Mater, 2016, 15: 564–569
25 Yang S, Li S, Song L, *et al.* Defect-density control of platinum-based nanoframes with high-index facets for enhanced electrochemical properties. Nano Res, 2019, 12: 2881–2888
26 Bu L, Shao Q, Huang X. Highly porous Pt-Pb nanostructures as active and ultrastable catalysts for polyhydric alcohol electrooxidations. Sci China Mater, 2019, 62: 341–350
27 Li HH, Fu QQ, Xu L, *et al.* Highly crystalline PtCu nanotubes with three dimensional molecular accessible and restructured surface for efficient catalysis. Energy Environ Sci, 2017, 10: 1751–1756
28 Wang H, Bai S, Pi Y, *et al.* A strongly coupled ultrasmall Pt_3Co nanoparticle-ultrathin $Co(OH)_2$ nanosheet architecture enhances selective hydrogenation of α,β-unsaturated aldehydes. ACS Catal, 2019, 9: 154–159
29 Chong L, Wen J, Kubal J, *et al.* Ultralow-loading platinum-cobalt fuel cell catalysts derived from imidazolate frameworks. Science, 2018, 362: 1276–1281
30 Wu Z, Bukowski BC, Li Z, *et al.* Changes in catalytic and adsorptive properties of 2 nm Pt_3Mn nanoparticles by subsurface atoms. J Am Chem Soc, 2018, 140: 14870–14877
31 Liu H, Liu K, Zhong P, *et al.* Ultrathin Pt–Ag alloy nanotubes with regular nanopores for enhanced electrocatalytic activity. Chem Mater, 2018, 30: 7744–7751
32 Tao Z, Chen W, Yang J, *et al.* Ultrathin yet transferrable Pt- or PtRu-decorated graphene films as efficient electrocatalyst for methanol oxidation reaction. Sci China Mater, 2019, 62: 273–282
33 Zhao F, Yuan Q, Luo B, *et al.* Surface composition-tunable octahedral PtCu nanoalloys advance the electrocatalytic performance on methanol and ethanol oxidation. Sci China Mater, 2019, 62: 1877–1887
34 Qi Z, Xiao C, Liu C, *et al.* Sub-4 nm PtZn intermetallic nanoparticles for enhanced mass and specific activities in catalytic electrooxidation reaction. J Am Chem Soc, 2017, 139: 4762–4768
35 Huang J, Liu Y, Xu M, *et al.* PtCuNi tetrahedra catalysts with tailored surfaces for efficient alcohol oxidation. Nano Lett, 2019, 19: 5431–5436
36 Wu F, Niu W, Lai J, *et al.* Highly excavated octahedral nanostructures integrated from ultrathin mesoporous $PtCu_3$ nanosheets: construction of three-dimensional open surfaces for enhanced electrocatalysis. Small, 2019, 15: 1804407
37 Qiu HJ, Xu HT, Li X, *et al.* Core–shell-structured nanoporous PtCu with high Cu content and enhanced catalytic performance. J Mater Chem A, 2015, 3: 7939–7944
38 Chen G, Zhao Y, Fu G, *et al.* Interfacial effects in iron-nickel hydroxide-platinum nanoparticles enhance catalytic oxidation. Science, 2014, 344: 495–499
39 Cao L, Zhao Z, Liu Z, *et al.* Differential surface elemental distribution leads to significantly enhanced stability of PtNi-based ORR catalysts. Matter, 2019, 1: 1567–1580
40 Huang L, Zhang W, Li P, *et al.* Exposing Cu-rich {110} active facets

in PtCu nanostars for boosting electrochemical performance toward multiple liquid fuels electrooxidation. Nano Res, 2019, 12: 1147–1153
41 Chang J, Song L, Xu Y, *et al.* Fishbone-like platinum-nickel nanowires as an efficient electrocatalyst for methanol oxidation. Nano Res, 2020, 13: 67–71
42 Zhang XF, Wang AJ, Zhang L, *et al.* Solvothermal synthesis of monodisperse PtCu dodecahedral nanoframes with enhanced catalytic activity and durability for hydrogen evolution reaction. ACS Appl Energy Mater, 2018, 1: 5054–5061
43 Niu HJ, Chen HY, Wen GL, *et al.* One-pot solvothermal synthesis of three-dimensional hollow PtCu alloyed dodecahedron nanoframes with excellent electrocatalytic performances for hydrogen evolution and oxygen reduction. J Colloid Interface Sci, 2019, 539: 525–532
44 Huang XY, Wang AJ, Zhang XF, *et al.* One-step synthesis of PtCu alloyed nanocages with highly open structures as bifunctional electrocatalysts for oxygen reduction and polyhydric alcohol oxidation. ACS Appl Energy Mater, 2018, 1: acsaem.8b01385
45 Zhang N, Shao Q, Wang P, *et al.* Porous Pt-Ni nanowires within *in situ* generated metal-organic frameworks for highly chemoselective cinnamaldehyde hydrogenation. Small, 2018, 14: 1704318
46 Fu G, Yan X, Cui Z, *et al.* Catalytic activities for methanol oxidation on ultrathin $CuPt_3$ wavy nanowires with/without smart polymer. Chem Sci, 2016, 7: 5414–5420
47 Teng X, Han WQ, Ku W, *et al.* Synthesis of ultrathin palladium and platinum nanowires and a study of their magnetic properties. Angew Chem Int Ed, 2008, 47: 2055–2058
48 Yan X, Chen Y, Deng S, *et al. In situ* integration of ultrathin PtCu nanowires with reduced graphene oxide nanosheets for efficient electrocatalytic oxygen reduction. Chem Eur J, 2017, 23: 16871–16876
49 Song P, Cui X, Shao Q, *et al.* Networked Pt–Sn nanowires as efficient catalysts for alcohol electrooxidation. J Mater Chem A, 2017, 5: 24626–24630
50 Ying J, Jiang G, Cano ZP, *et al.* Spontaneous weaving: 3D porous PtCu networks with ultrathin jagged nanowires for highly efficient oxygen reduction reaction. Appl Catal B-Environ, 2018, 236: 359–367
51 Pei J, Mao J, Liang X, *et al.* Ultrathin Pt–Zn Nanowires: High-performance catalysts for electrooxidation of methanol and formic acid. ACS Sustain Chem Eng, 2018, 6: 77–81
52 Cheng D, Wu D, Xu H, *et al.* Composition-controlled synthesis of PtCuNPs shells on copper nanowires as electrocatalysts. ChemistrySelect, 2016, 1: 4392–4396
53 Xu Y, Cui X, Wei S, *et al.* Highly active zigzag-like Pt-Zn alloy nanowires with high-index facets for alcohol electrooxidation. Nano Res, 2019, 12: 1173–1179
54 Huang L, Zhang X, Wang Q, *et al.* Shape-control of Pt–Ru nanocrystals: tuning surface structure for enhanced electrocatalytic methanol oxidation. J Am Chem Soc, 2018, 140: 1142–1147
55 Fujita T, Guan P, McKenna K, *et al.* Atomic origins of the high catalytic activity of nanoporous gold. Nat Mater, 2012, 11: 775–780
56 Bu L, Ding J, Guo S, *et al.* A general method for multimetallic platinum alloy nanowires as highly active and stable oxygen reduction catalysts. Adv Mater, 2015, 27: 7204–7212
57 Xu X, Zhang X, Sun H, *et al.* Synthesis of Pt-Ni alloy nanocrystals with high-index facets and enhanced electrocatalytic properties. Angew Chem Int Ed, 2014, 53: 12522–12527
58 Tian N, Zhou ZY, Sun SG. Platinum metal catalysts of high-index surfaces: From single-crystal planes to electrochemically shape-controlled nanoparticles. J Phys Chem C, 2008, 112: 19801–19817
59 Yang L, Song X, Qi M, *et al.* Templated high-yield synthesis of Pt nanorods enclosed by high-index {311} facets for methanol selective oxidation. J Mater Chem A, 2013, 1: 7316–7320
60 Zhang N, Bu L, Guo S, *et al.* Screw thread-like platinum–copper nanowires bounded with high-index facets for efficient electrocatalysis. Nano Lett, 2016, 16: 5037–5043
61 Huang X, Zhao Z, Fan J, *et al.* Amine-assisted synthesis of concave polyhedral platinum nanocrystals having {411} high-index facets. J Am Chem Soc, 2011, 133: 4718–4721
62 Chen Y, Yuan PX, Wang AJ, *et al.* A novel electrochemical immunosensor for highly sensitive detection of prostate-specific antigen using 3D open-structured PtCu nanoframes for signal amplification. Biosens Bioelectron, 2019, 126: 187–192
63 Li K, Li X, Huang H, *et al.* One-nanometer-thick PtNiRh trimetallic nanowires with enhanced oxygen reduction electrocatalysis in acid media: integrating multiple advantages into one catalyst. J Am Chem Soc, 2018, 140: 16159–16167
64 Greeley J, Mavrikakis M. Competitive paths for methanol decomposition on Pt(111). J Am Chem Soc, 2004, 126: 3910–3919
65 Lu X, Deng Z, Guo C, *et al.* Methanol oxidation on $Pt_3Sn(111)$ for direct methanol fuel cells: methanol decomposition. ACS Appl Mater Interfaces, 2016, 8: 12194–12204

Acknowledgements We acknowledge the financial support from the National Natural Science Foundation of China (21571001, 21631001, and U1532141), the Ministry of Education, and the Education Department of Anhui. Zhang W and Wang YG gratefully acknowledge the financial support by Guangdong Provincial Key Laboratory of Catalysis, Southern University of Science and Technology (SUSTech), China (2020B121201002), and the computational resource support from the Center for Computational Science and Engineering at SUSTech.

Author contributions Huang L and Zhong Y performed the experiments and did some characterizations. Xiang D, Yuan X and Wang D analyzed and discussed the data. Wang YG and Zhang W performed the DFT calculations and theoretical analyses. Huang L wrote the manuscript with support from Li P, Li X and Uddin W. Li P and Zhu M designed the study and supervised the project. All authors contributed to the general discussion.

Conflict of interest The authors declare that they have no conflict of interest.

Supplementary information Supporting data are available in the online version of the paper.

Liping Huang obtained her BSc degree from Hebei Normal University in 2017. She is currently a Master candidate under the supervision of Prof. Peng Li at Anhui University. Her research interest focuses on the electrocatalysis of noble metal nanomaterials.

Peng Li is a professor at Anhui University. He received his PhD degree in chemistry from Tsinghua University in 2011. He was a visiting scholar at the University of California at Los Angeles (UCLA) from 2016 to 2017. His current research interests focus on the syntheses of metallic nanomaterials and metal nanoclusters, and their applications in energy conversion and catalysis.

Yang-Gang Wang received his PhD degree from Tsinghua University in 2014 under the supervision of Prof. Jun Li. From 2014 to 2016, he worked as a postdoctoral Research Associate at Pacific Northwest National Laboratory (USA) with Dr. Roger Rousseau and Dr. Vanda Glezakou. After that, he worked as an Alexander von Humbold Fellow at Fritz Haber Institute (Germany) with Dr. Sergey Levchenko and Prof. Matthias Scheffler from 2016 to 2018. He currently works at Southern University of Science and Technology as an associate professor. His research interests focus on theoretical and computational heterogeneous catalysis.

超细PtCu纳米线的表面结构调控及其增强的醇类电催化氧化作用

黄莉萍[1,2†], 张伟[3,4†], 钟艳飞[1,2†], 李鹏[1,2*], 项东[1], Waqar Uddin[1], 李小武[1], 王阳刚[3*], 袁孝友[1], 王定胜[5], 朱满洲[1,2*]

摘要 铂基纳米催化剂的表面结构调控是提升其电催化性能和实现多功能性的有效途径. 本工作报道了两种超细PtCu纳米线(光滑型和粗糙型)的湿化学合成方法及其电催化醇氧化的性能. 研究结果表明, 粗糙型PtCu合金表面具有丰富的原子台阶, 对多种电化学反应具有较好的催化活性. 密度泛函理论模拟表明, 粗糙型PtCu纳米线具有较好的反应活性, 这是由于Pt-Cu位点之间的协同作用促进了反应过程中水的解离和羧基中间体的脱氢. 本工作为能源相关电催化体系中合金纳米催化剂的合理设计提供了思路.

